Dynamics of component exchange at PML nuclear bodies

Stefanie Weidtkamp-Peters[1,*], Thorsten Lenser [2,*], Dmitri Negorev[3], Norman Gerstner[1], Thomas G. Hofmann[4], Georg Schwanitz[1], Christian Hoischen[1], Gerd Maul[3], Peter Dittrich[2] and Peter Hemmerich[1,‡]

[1]Leibniz-Institute of Age Research, Fritz-Lipman-Institute, Beutenbergstr. 11, 07745 Jena, Germany
[2]Institute of Computer Science, Friedrich-Schiller-University, 07743 Jena, Germany
[3]The Wistar Institute, 3601 Spruce Street, Philadelphia, PA 19104, USA
[4]German Cancer Research Center, Im Neuenheimer Feld 242, 69120 Heidelberg, Germany
*These authors contributed equally to this work
‡Author for correspondence (e-mail: phemmer@fli-leibniz.de)

Accepted 27 May 2008
Journal of Cell Science 121, 2731-2743 Published by The Company of Biologists 2008
doi:10.1242/jcs.031922

Summary

PML nuclear bodies (NBs) are involved in the regulation of key nuclear pathways but their biochemical function in nuclear metabolism is unknown. In this study PML NB assembly dynamics were assessed by live cell imaging and mathematic modeling of its major component parts. We show that all six nuclear PML isoforms exhibit individual exchange rates at NBs and identify PML V as a scaffold subunit. SP100 exchanges at least five times faster at NBs than PML proteins. Turnover dynamics of PML and SP100 at NBs is modulated by SUMOylation. Exchange is not temperature-dependent but depletion of cellular ATP levels induces protein immobilization at NBs. The PML-RARα oncogene exhibits a strong NB retention effect on wild-type PML proteins. HIPK2 requires an active kinase for PML NB targeting and elevated levels of PML IV increase its residence time. DAXX and BLM turn over rapidly and completely at PML NBs within seconds. These findings provide a kinetics model for factor exchange at PML NBs and highlight potential mechanisms to regulate intranuclear trafficking of specific factors at these domains.

Supplementary material available online at
http://jcs.biologists.org/cgi/content/full/121/16/2731/DC1

Key words: Nuclear body, Promyelocytic leukemia, SP100, SUMO, RARα, Assembly, Kinetics modeling, FRAP, FCS

Introduction

Beside chromosome territories, the mammalian nucleus contains a variety of internal domains, such as nucleoli, speckles, Cajal bodies and promyelocytic leukemia nuclear bodies (PML NBs) (Lamond and Earnshaw, 1998). These structures form a dynamic framework that is able to change the functional organization of the nucleus during the cell cycle or upon external signals in order to fulfill or support biochemical activities on chromatin (Lanctot et al., 2007). Whereas nucleoli, speckles and Cajal bodies are devoted to ribosome biogenesis, splicing factor sequestration and snRNP maturation, respectively (Hemmerich and Diekmann, 2005), the biochemical function of PML NBs is still unclear (Bernardi and Pandolfi, 2007). PML NBs, also known as nuclear domain 10 (ND10) are macromolecular protein assemblies in the nucleus of mammalian cells that range in size from 0.3-1.0 μm in diameter (Maul et al., 2000). Depending on cell type, cell cycle and cell condition, the number and distribution of PML NBs can vary considerably but is typically between 10 and 20 (Ascoli and Maul, 1991; Maul et al., 1995). Electron microscopy revealed a ring-like shape of PML NBs consisting of a fibrillar sphere that surrounds a central core (Dyck et al., 1994; Weis et al., 1994; Boisvert et al., 2000). Normal PML NBs do not contain DNA or RNA, but chromatin threads and RNA or RNPs are in contact with the surface of the bodies (Boisvert et al., 2000; Kiesslich et al., 2002; Eskiw et al., 2004).

The signature protein of PML NBs is the promyelocytic leukemia gene product PML (Daniel et al., 1993). PML is expressed in all mammalian tissues and cell lines reported (Gambacorta et al., 1996). Several PML isoforms that vary in their C-termini and subcellular distribution are expressed from alternatively spliced PML transcripts (Jensen et al., 2001). Cells that lack PML are unable to form NBs and other PML NB components show a dispersed nuclear distribution (Ishov et al., 1999). In acute promyelocytic leukemia (APL) the gene expressing the retinoic acid receptor α (*RARα*, also known as RARA) is fused to the gene encoding the PML protein by a reciprocal t(15;17) chromosomal translocation (de Thé et al., 1990; Goddard et al., 1991). Expression of PML-RARα induces leukemia and disrupts PML NBs into a microspeckled localization pattern in APL blasts as a consequence of a dominant-negative effect of PML-RARα through direct physical interaction with wild-type PML (reviewed in Melnick and Licht, 1999). Administration of retinoic acid reverses this aberrant phenotype, resulting in the reformation of NBs and clinical remission of APL patients (Koken et al., 1994).

Immunofluorescence analyses identified proteins that are either constitutively or conditionally associated with this structure. Proteins present at PML NBs at endogenous expression levels include SP100, DAXX, the Bloom syndrome gene product (BLM), the small ubiquitin-related modifier 1 (SUMO1), and NDP55 (Negorev and Maul, 2001). SUMO has an important role in regulating the distribution of SUMO-modified proteins between PML NBs and the nucleoplasm (Seeler and Dejean, 2001). The formation of NBs relies primarily on the self-assembly abilities of the N-terminal

RBCC domain in PML (Reymond et al., 2001). In vitro, the bacterially expressed, non-SUMOylated RBCC domain forms spherical structures with remarkable similarity to nuclear PML bodies (Kentsis et al., 2002). Deletions or mutations within this domain abrogate NB formation and the transformation-suppressive effect of PML in vivo (Le et al., 1996; Borden, 2002). PML harbors three SUMOylation sites (Kamitani et al., 1998), and SUMOylation of PML is essential for the formation of normal NBs in mammalian cells (Ishov et al., 1999; Zhong et al., 2000). In addition, PML and other PML NB components, such as SP100 and DAXX, contain a SUMO-binding motif (SBM) with which these proteins can bind SUMO noncovalently (Song et al., 2004). Binding of proteins to NBs can therefore be modulated by noncovalent interactions between the SUMO moieties and SBMs of PML NB components (Shen et al., 2006; Lin et al., 2007).

Currently, the nuclear protein database lists 78 proteins that have been reported to localize at PML NBs (http://npd.hgu.mrc.ac.uk/index.html). These proteins and, by inference, the NBs, are functionally implicated in a variety of cellular processes, including apoptosis, DNA damage response, cellular senescence and angiogenesis (reviewed in Bernardi and Pandolfi, 2007). This functional heterogeneity has made it difficult to propose a single function for PML NBs (Borden, 2002; Bernardi and Pandolfi, 2007). The NBs might be directly involved in these processes by modulating chromatin structure, regulating transcription of specific genes, sequestering nuclear proteins and/or mediating posttranslational modifications of specific target proteins (Bernardi and Pandolfi, 2007). Inherent to all these models is the question whether PML NB components function directly within this structure or somewhere outside at different intranuclear sites, or both. A regulated network traffic between these sites may constitute a potential control mechanism with PML at its core (Ishov et al., 1999).

In this study, we have analyzed the complexity and plasticity of this supramolecular regulatory mechanism by assessing the full range of intranuclear mobilities of eleven GFP-tagged PML NB components and derivatives by a combination of fluorescence recovery after photobleaching (FRAP), fluorescence correlation spectroscopy (FCS), and mathematic modeling.

Results

GFP-tagged PML isoforms are functional

The six nuclear isoforms of the PML protein result from extensive alternative splicing of exon 7 to exon 9 (Fig. 1A) (Jensen et al., 2001). To study their nuclear dynamics we fused them to GFP. For live-cell experiments, the GFP-tagged PML isoforms were transiently transfected into U-2 OS, HEp-2 or HeLa cells. All fusion constructs were expressed as full-length proteins (supplementary material Fig. S1A). Endogenous PML protein expression in U-2 OS cells was identical to that in MRC-5 cells (supplementary material Fig. S1B), which express all six nuclear PML isoforms (Condemine et al., 2006). We therefore used U-2 OS cells, but would like to point out that similar results were obtained for HEp-2 and HeLa cells that also showed similar isoform expression patterns in western blots (data not shown). Immunolocalization confirmed that all six GFP-tagged PML isoforms localize to SP100-containing NBs and are expressed at low levels (supplementary material Fig. S2A). These were identical to PML bodies of untransfected cells with respect to size and number in all cell lines analyzed (our unpublished data). Cells with minimal expression levels of the fusion proteins were generally chosen for live cell experiments. To test whether

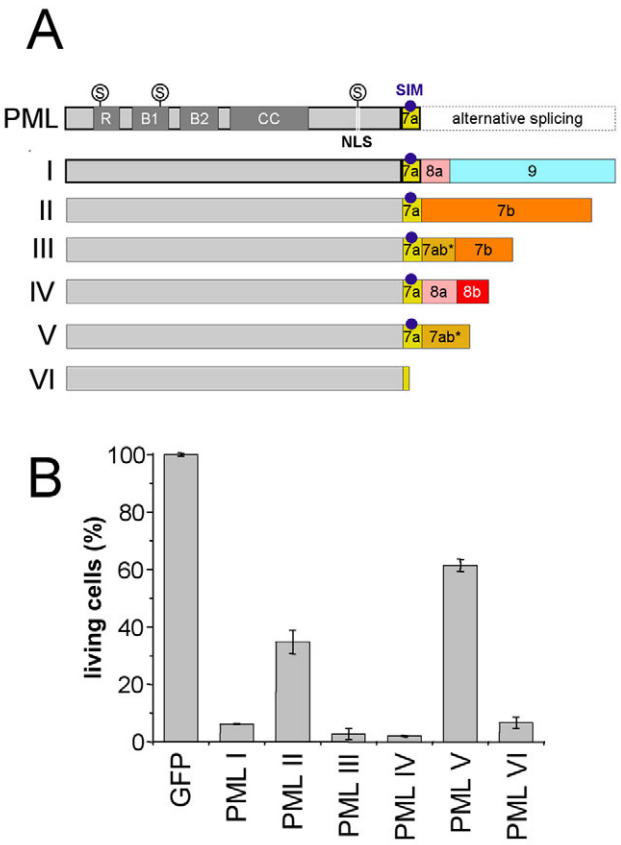

Fig. 1. GFP-PML isoforms are biologically active as growth suppressors. (A) Schematic depiction of the domain structure of PML isoforms (Jensen et al., 2001). All PML isoforms share a common N terminus but differ in their C termini, attributable to the alternative splicing of exons 7 to 9. Protein domains of all PML isoforms include the RING finger (R), the B1 and B2 boxes, the coiled-coil motif (CC), a nuclear localization signal (NLS) and three SUMOylation sites (S). PML VI does not contain the SUMO interacting motif (SIM) within exon 7a. (B) U-2 OS cells were transiently transfected with equal amounts of plasmids expressing GFP, or GFP–PML-I, GFP–PML-II, GFP–PML-III or GFP–PML-VI. Four days after transfection the number of living cells was determined by Trypan-Blue exclusion and normalized to GFP-expressing cells. The diagram shows mean values ± s.d. of three independent experiments.

the GFP-PML constructs are functional, we analyzed their cell-growth-suppressive capacity (Mu et al., 1994) in transient transfection assays. This demonstrated that all six GFP-tagged PML isoforms were functional as cell growth suppressors (Fig. 1B). Interestingly, although the transfection efficiency was the same for all constructs (70-80% after 24 hours, our unpublished data) they differed in their efficiency to suppress cell growth (Fig. 1B).

Protein-specific exchange dynamics of PML isoforms at NBs

To investigate the turnover of individual PML isoforms at NBs we employed FRAP. A spherical region containing one PML NB was bleached to background levels and fluorescence recovery was monitored for 20 minutes (Fig. 2). FRAP at bleached NBs was substantially different between the isoforms. Whereas, for example, a considerable amount of GFP–PML-I fluorescence had already recovered after 5 minutes, there was only little recovery in GFP–PML-V-expressing cells after that time (Fig. 2A). FRAP curves confirmed that all PML proteins exhibited individual

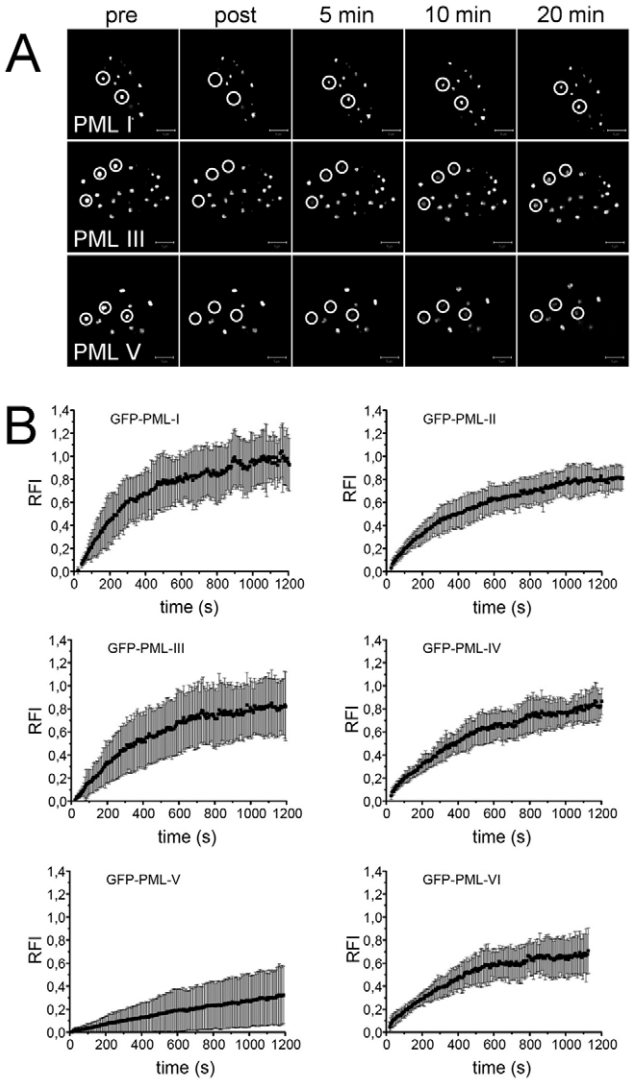

Fig. 2. Exchange of PML isoforms at NBs. (A) FRAP experiments were performed on U-2 OS cells that express the indicated GFP-tagged PML isoforms by bleaching circled areas that contain an NB (pre, before bleach pulse; post, immediately after the bleach pulse) and monitoring fluorescence recovery for 20 minutes. Scale bars, 5 µm. (B) Quantification of FRAP experiments for each isoform. The graphs show mean values (± s.d. from at least 20 FRAP experiments each) as relative fluorescence intensity (RFI) after normalization to prebleach levels.

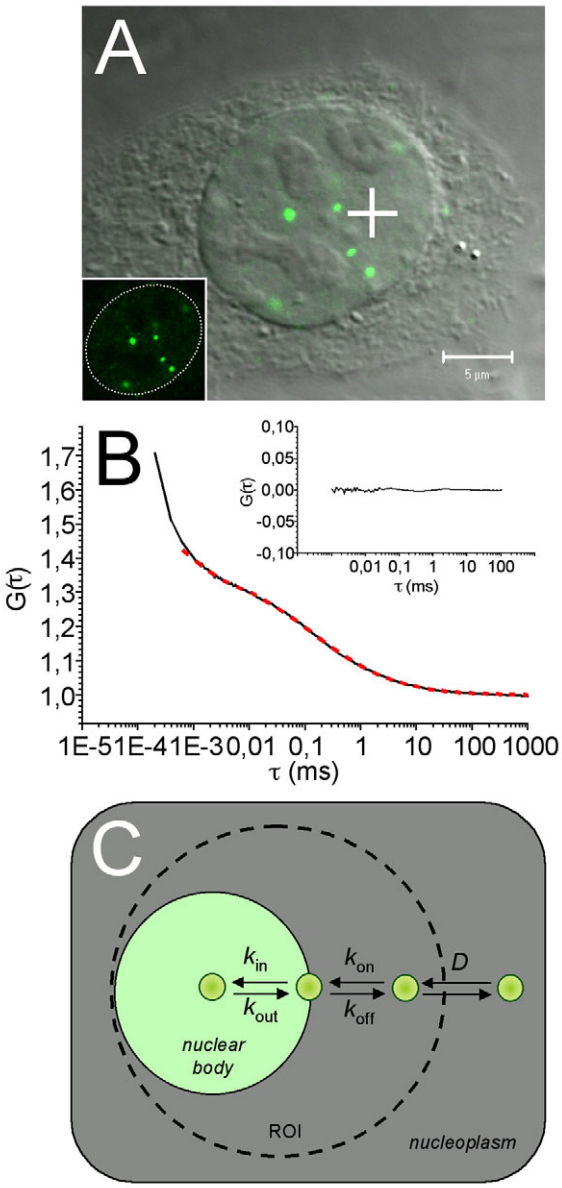

Fig. 3. Diffusion behavior of PML protein isoforms outside NBs. (A) U-2 OS cell expressing GFP–PML-IV (green) merged with the respective DIC image before FCS measurement. The inset shows only the GFP signals within the nucleus (indicated by dotted line) of this cell. +, position of the FCS laser beam. Scale bar, 5 µm. (B) Mean autocorrelation data obtained from FCS-count-rate traces for GFP–PML-IV-expressing cells (solid black line). Data were fitted using an anomalous diffusion model (dashed red line). The inset graph displays a residual plot from the fit. (C) Kinetics modeling of PML NB assembly according to a diffusion-binding model. Molecules with the potential to accumulate at PML NBs move by diffusion (*D*) in the nucleoplasm outside NBs. Upon stochastic encounter, molecules associate and dissociate from the periphery of the NB (k_{on} and k_{off}, respectively) and penetrate into and out of the core of the NB (k_{in} and k_{out}, respectively). Dashed circle, ROI for bleaching and recovery measurements employed in FRAP experiments.

exchange dynamics at NBs (Fig. 2B). Most strikingly, GFP–PML-V showed an almost linear increase of fluorescence, and recovery reached only 32% after 20 minutes (Fig. 2E). Thus, PML V is the most stable isoform, suggesting that it serves as a scaffold component of PML NBs.

PML protein mobility outside NBs is governed by anomalous diffusion

To test whether the exchange dynamics of PML proteins depend on their mobility in the nucleoplasm we applied FCS (Weidtkamp-Peters et al., 2008). Using this technique we were able to directly assess the diffusion coefficient (*D*) of the nucleoplasmic pools of nls-GFP-tagged PML protein isoforms and all other NB components analyzed in this study (Fig. 3A,B; Table 1). The *D* value of nls-GFP alone in the nucleus was 9.5±1.5 µm^2 seconds^{-1}, which is in perfect agreement with independent measurements (Wachsmuth et al., 2000). This *D* value is well below the one of GFP measured by FCS or FRAP in solution (*D*=~90 µm^2 seconds^{-1}) (Swaminathan et al.,1997; Hink et al., 2000), hence reflecting anomalous diffusion of untagged GFP in the crowded nuclear environment. The *D* values

of PML isoforms, however, were significantly smaller than for nls-GFP. They ranged from 1.02±0.11 μm^2 seconds^{-1} for PML II to 2.79±0.11 μm^2 seconds^{-1} for PML V (Table 1). These *D* values are too low to account only for diffusion barriers based on the size of the fusion proteins compared with GFP. Evaluation of the FCS data also delivered the anomaly parameter (α), which describes the degree of obstruction for diffusing particles by the medium (Saxton, 2001). Under conditions of free diffusion, i.e. in buffer solutions, α equals 1, but decreases continuously to a limit value of α=0.75 for GFP with increasing crowding conditions and obstacle concentration (Banks and Fradin, 2005). Compatible with this assumption we found α=0.73 for nls-GFP alone, but substantially lower values for PML isoforms and all other PML NB components (Table 1). The low *D* values and anomaly parameters, therefore, strongly indicate transient binding events of PML components with chromatin or protein-based complexes throughout the nuclear volume. We conclude that this diffusion behavior, although anomalous, grants similarly free access of all PML NB components to NBs.

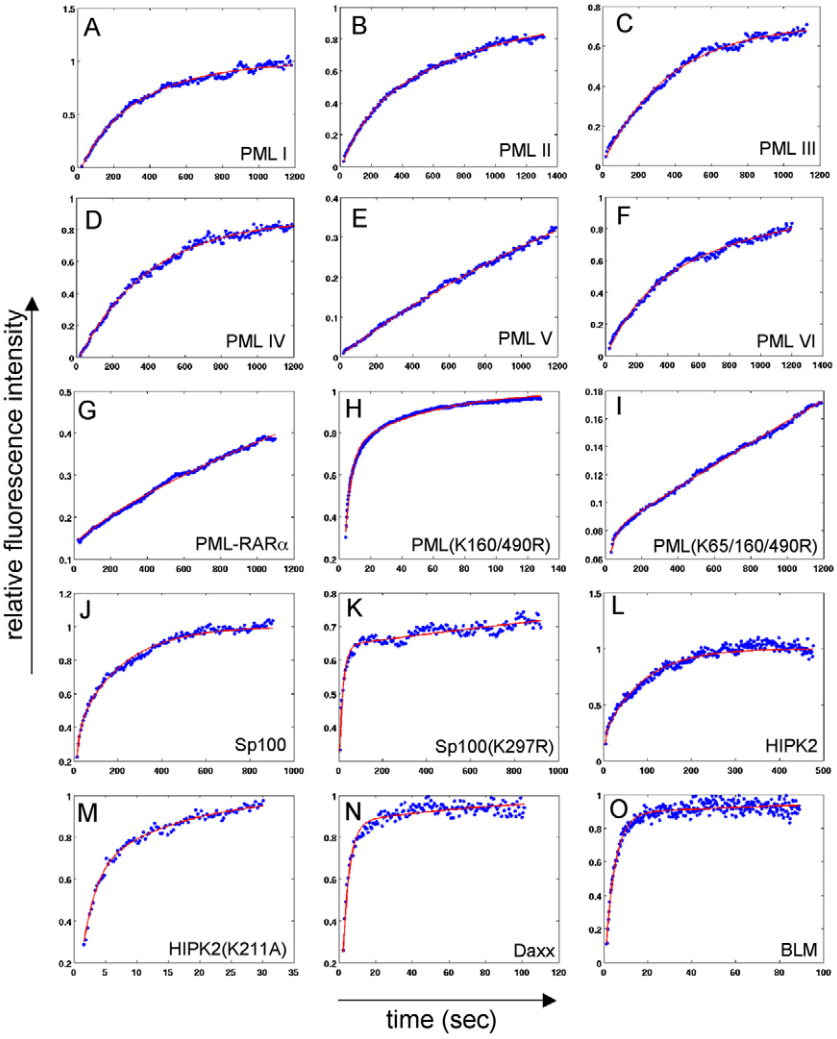

Fig. 4. (A-O) Fitting of FRAP data with the diffusion-binding model. The mean values of FRAP curves for the indicated GFP-tagged proteins (blue dots) were fitted using the diffusion-binding model depicted in Fig. 3C. Fit curves are shown as solid red lines. Note that these fits also consider the individual *D* values of PML isoforms derived from FCS measurements.

A binding-diffusion model to describe component exchange at PML NBs

On the basis of the FRAP and FCS results we developed a binding-diffusion model for the quantitative description of protein exchange at these structures (Sprague and McNally, 2005) (Fig. 3C). Diffusion inside and out bleached regions was modeled as a linear two-way process using the measured *D* values in FCS experiments as described in Materials and Methods. Table 1 contains for each of the PML NB components the *D* values and anomaly parameters α, the binding and unbinding rates k_{on} and k_{off}, and the rates of movement to the inner core and to the outer surface of the body k_{in} and k_{out}, respectively. From these, we computed the residence time (Rt), i.e. the mean time a molecule spends bound to the NB, and the fraction of molecules bound in the inner and outer region of the body, bnd_{in} and bnd_{out}, respectively. Conceptually, this model can also be applied to proteins with short Rt values, since these may split into two populations, one which immediately dissociates after surface contact with rate constants k_{on} and k_{off}, and a second which encounters additional binding partners at or in the nuclear body with rate constants k_{in} and k_{out}. We therefore applied this binding-diffusion model to all PML NB components analyzed in this study. This model provided good fits to the measured FRAP curves of all PML components (Fig. 4). A binding-diffusion model assuming that all molecules exchange with the same rate did not result in good fits (supplementary material Fig. S3). Moreover, FRAP curves could never be fitted well with one-component exponential functions (T.L. and P.H., unpublished results). These observations confirmed the existence of at least two differently mobile populations of molecules at NBs.

SUMO conjugation modulates exchange rates of PML at NBs

SUMO can be covalently conjugated to PML at lysine residues 65, 160 and 490 (Kamitani et al., 1998). We therefore wondered whether PML exchange at NBs would be affected by the SUMOylation pattern of PML. To test this, we used the two PML variants SUMO-2K and SUMO-3K, which contain lysine-to-arginine mutations at positions 160 and 490, and 65,160 and 490, respectively (Fig. 5A). GFP–PML–SUMO-2K localized to PML NBs, but in contrast to wild-type PML, the nucleoplasmic fluorescence was substantially increased (supplementary material Fig. S2B), thus indicating weaker binding to NBs, stronger retention within chromatin, or both. FRAP analysis revealed fast recovery kinetics of GFP–PML–SUMO-2K in both the NBs and the nucleoplasm (Fig. 5B). Furthermore, GFP–PML–SUMO-2K fluorescence recovered rapidly and completely within 2 minutes at NBs (Fig. 5G). Quantitatively, the Rt of the GFP–PML–SUMO-2K (5.8 s) was reduced ~80 times compared with wild-type PML-IV (453 seconds, Table 1). Thus, SUMOylation of Lys60 and/or Lys490 is required for retention of PML at NBs. To test whether the reduced exchange rate results from an impaired ability to oligomerize, we expressed the mutant construct together with monomeric red fluorescent protein (mRFP)-tagged wild-type PML. This co-expression resulted in (1) a redistribution

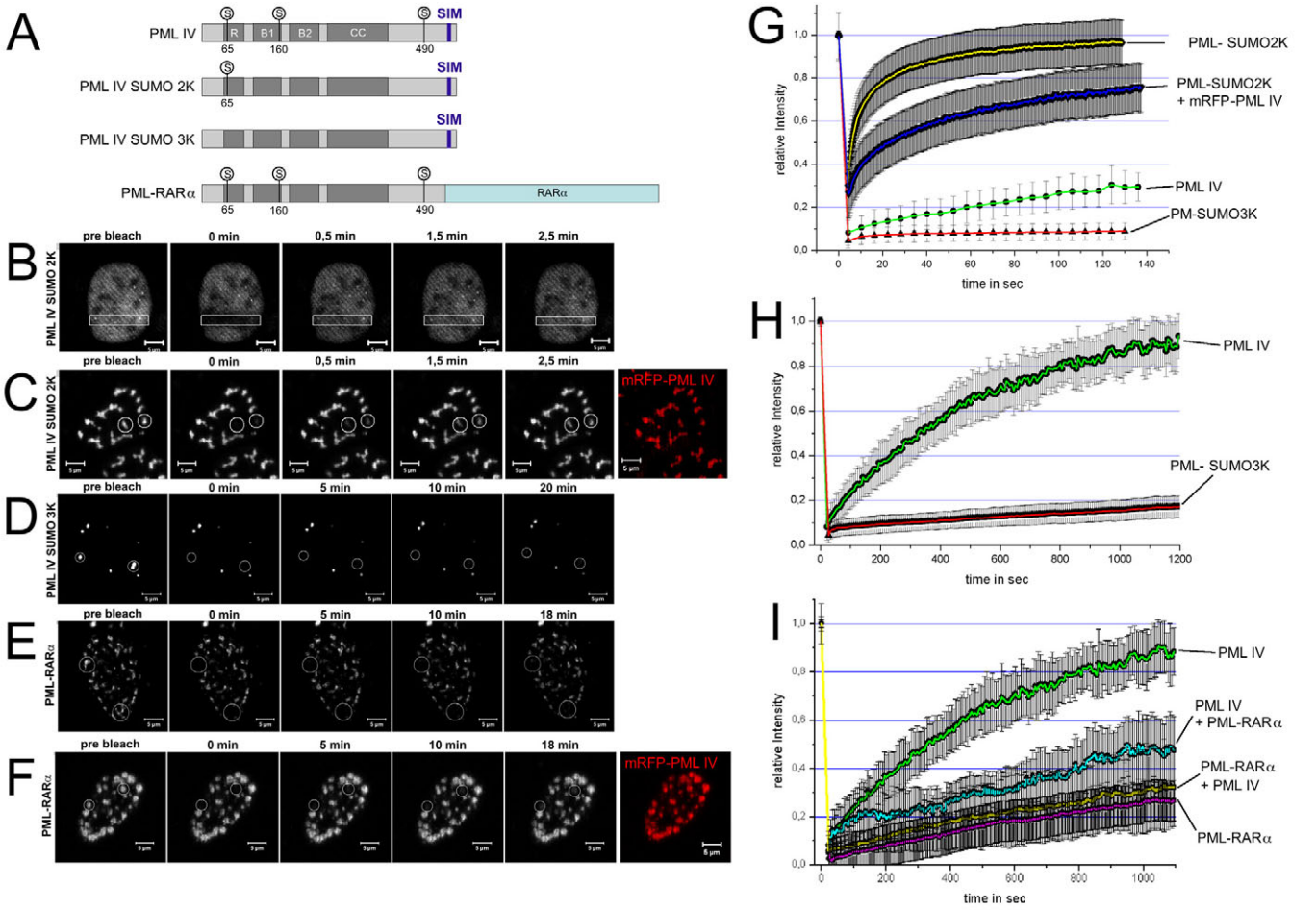

Fig. 5. Exchange of PML protein variants at NBs. (A) Schematic depiction of PML-fusion proteins used for FRAP experiments. The domain structure is as described in Fig. 1. SUMO-modifiable lysine residues at positions 65, 160 and 490 in PML are also shown. (B-F) U-2 OS cells transfected with the indicated GFP-tagged PML protein constructs were used in FRAP analyses of areas that contain NBs and fluorescence recovery was monitored for various times as indicated. Scale bars, 5 μm. In C and F, cells were co-transfected with PML IV tagged to mRFP in order to analyze the impact of wild-type PML on the exchange dynamics of PML-IV–SUMO-2K (C) and PML-RARα (F). (G-I) Graphs show mean values (± s.d.) from at least 20 FRAP experiments each, of the indicated proteins or protein combinations as relative fluorescence intensity (RFI) after normalization to pre-bleach levels.

of nucleoplasmic GFP–PML–SUMO-2K into NBs (Fig. 5C) and, (2) in substantially reduced FRAP kinetics (Fig. 5G). At the same time there was no difference in the nucleoplasmic diffusion behavior of GFP–PML–SUMO-2K compared with wild-type PML IV (Table 1). We therefore conclude that GFP–PML–SUMO-2K is still able to interact with other PML isoforms but that SUMOylation of Lys160 and/or Lys490 is required for the correct PML retention at NBs. GFP–PML–SUMO-3K localized to NBs without increased nucleoplasmic localization (Fig. 4D and 3; Fig. 5D), and turned over at PML NBs only very slowly (Fig. 5D and 5H), with a mean Rt of ~25 minutes (Table 1). Concomitantly, the fraction of more tightly NB-bound GFP–PML–SUMO-3K molecules (bnd_{in}) increased to 98%, which is more than threefold compared with wild-type PML IV (Table 1). Thus, the lack of SUMO moieties at positions Lys65, Lys160 and Lys490 results in a highly increased NB retention ability of PML in interphase cells.

Immobilization of wild-type PML in NBs by oncogenic PML-RARα

Previous FRAP analyses has shown that the intranuclear mobility of GFP-tagged PML-RARα oncoprotein is not much different from GFP-PML over short observation times (Dong et al., 2004; Huang et al., 2007). We were interested to know whether this is true for longer observation periods in FRAP experiments. As expected, GFP-PML-RARα localized in a microspeckled pattern containing PML and SP100 (supplementary material Fig. S2B) (Dong et al., 2004). FRAP revealed only very slow recovery of GFP-PML-RARα when observed over a period of 20 minutes (Fig. 5E,I). Quantitatively, we compared PML-RARα with PML VI, which is the shortest and also lacks the SIM domain (Fig. 5A). Fitting of the FRAP data with the binding-diffusion model revealed a mean Rt of GFP-PML-RARα at remaining NBs of ~38 minutes compared with ~8.8 minutes for PML VI (Table 1), accompanied by an increase of the more stably bound fraction of molecules from ~30% (PML VI) to ~76% (PML-RARα) (Table 1). Thus, the PML-RARα oncoprotein is a much more stable component of NBs than previously thought. To test whether this hyperstable binding of PML-RARα to NBs has an impact on other NB components, we determined FRAP recovery of PML IV in cells that were co-transfected with PML-RARα (Fig. 5I). This experiment revealed a marked decrease in GFP–PML-IV exchange rates at NBs in the presence of PML-RARα, whereas exchange of GFP-PML-RARα remained unchanged (Fig. 5I). GFP-PML-RARα

also reduced the exchange kinetics of other GFP-tagged isoforms upon coexpression (data not shown). These observations demonstrate that the PML-RARα oncoprotein has a dominant NB-retention effect on wild-type PML proteins.

Exchange dynamics of SP100 at PML NBs

SP100 is a PML NB constituent with potential functions in transcriptional regulation at promoters of specific genes (Sternsdorf et al., 2005). Protein domains identified in SP100 include a homo-oligomerization and an NB-targeting domain, an HP1-binding domain containing a SUMOylation site at Lys297, and an NLS (Fig. 6A) (Sternsdorf et al., 1999; Negorev et al., 2001). GFP-tagged SP100 wild-type and variant proteins as depicted in Fig. 5A localized to PML NBs and were expressed as full-length proteins (supplementary material Fig. S2C). Exchange rates of these proteins were analyzed by FRAP analysis (Fig. 6B). Quantification was done by using the binding-diffusion model, and showed that SP100 exchanged at NBs more than five times faster than the fastest PML isoform (Rt values of ~48 seconds vs ~272 seconds, respectively) and fluorescence recovered completely after ~10 minutes (vs >20 minutes in the case of PML I) (Fig. 6D; Table 1). Mutation of the SUMOylation site in SP100 resulted in faster than wild-type recovery kinetics (within seconds) but much slower recovery (within minutes; (Fig. 6C). This observation indicates two distinct populations of molecules that can be quantified by the diffusion-binding model: whereas the k_{on} and k_{off} values were similar to wild-type SP100, k_{in} and k_{out} were reduced ~30 and ~20 times, respectively (Table 1). In other words, binding and unbinding of non-SUMOylated SP100 at the periphery of PML NBs is unaltered, whereas incorporation into the core becomes much more efficient when SP100 is not SUMOylated. We re-addressed this observation by testing several deletion variants. A C-terminal deletion variant that still contains the SUMOylation site (SP100 1-332) shows almost wild-type exchange rates, whereas all other deletion variants that lack the SUMOylation site show strong or complete immobilization at PML NBs (Fig. 6D). Thus, SUMOylation does not influence the binding of SP100 to NBs but it affects its incorporation into the core. A GFP construct containing only the oligomerization domain of SP100 (aa 29-152) was completely immobile at PML NBs (Fig. 6D), and its Rt, as derived from the binding-diffusion model, was 10.3 hours.

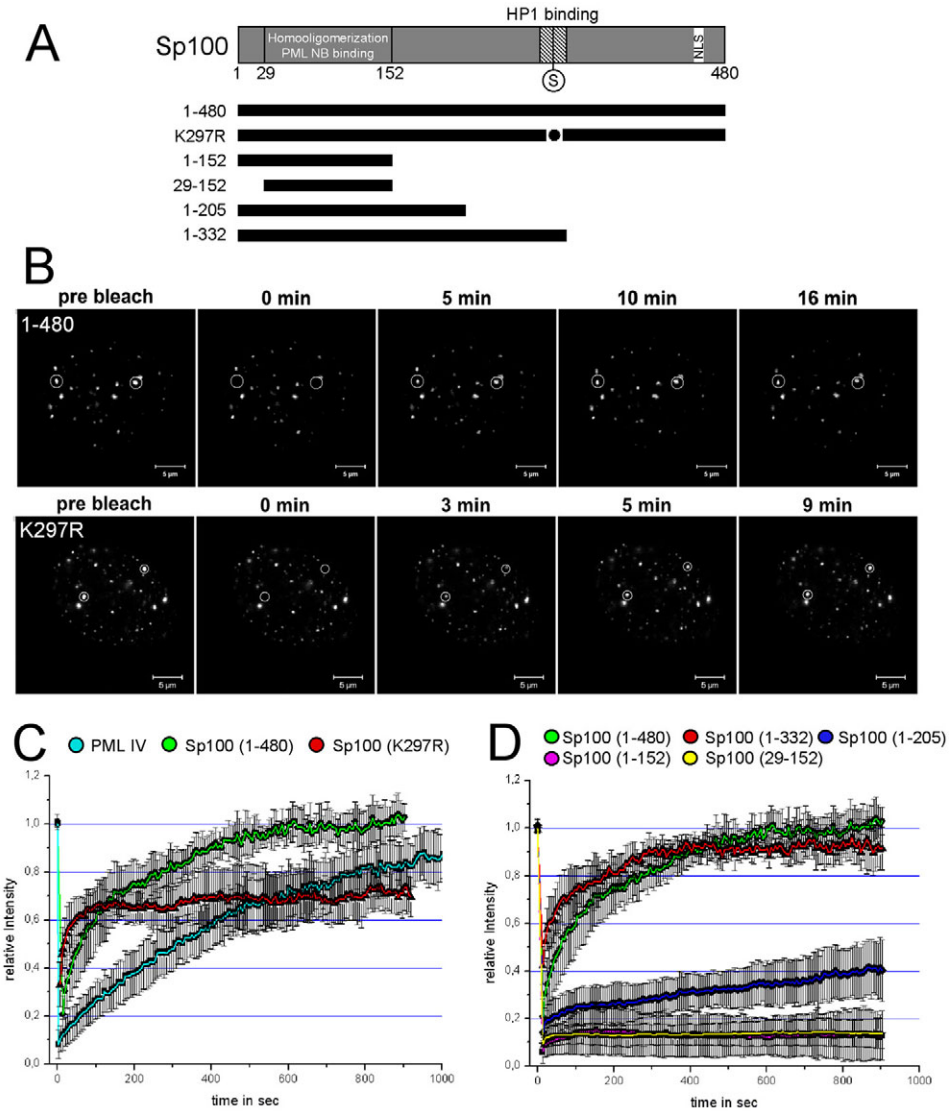

Fig. 6. Exchange dynamics of SP100 and SP100 mutant constructs at NBs. (A) Schematic depiction of SP100 protein and mutants used for FRAP analyses. The oligomerization and PML NB targeting resides within a region spanning amino acids 29-152 of SP100 (Negorev et al., 2001). SP100 has a SUMOylation site at Lys297 (S) within the HP1-binding motif and a nuclear localization signal at the C-terminus (NLS). Note, that SP100 variants that lack the endogenous NLS were engineered to contain one at their N-termini (Negorev et al., 2001). (B) FRAP experiments were performed in U-2 OS cells that express GFP-tagged SP100 wild-type (aa 1-480) and the indicated variants, by bleaching areas that contain NBs and by monitoring fluorescence recovery for various intervals as indicated. Scale bars, 5 μm. (C,D) Quantification of FRAP experiments as shown in B. Graphs show mean values (± s.d.) from at least 20 FRAP experiments. For comparison, the FRAP curve of GFP–PML-IV at NBs was included in C.

HIPK2 binding to PML NBs requires kinase activity and its exchange is modulated by PML IV

HIPK2 is a kinase involved in cell proliferation and apoptosis by phosphorylation-induced stabilization of the tumor suppressor p53 (Hofmann et al., 2002; D'Orazi et al., 2002). In U-2 OS cells, GFP-tagged HIPK2 distributes uniformly throughout the nucleoplasm and accumulates at PML NBs, in agreement with previous localization studies (supplementary material Fig. S2D) (Hofmann et al., 2002). Modeling of the FRAP data revealed an Rt value of 11 seconds for GFP-HIPK2 at PML NBs indicating a fast turnover (Fig. 7A,F; Table 1). We then analyzed HIPK2 dynamics at NBs

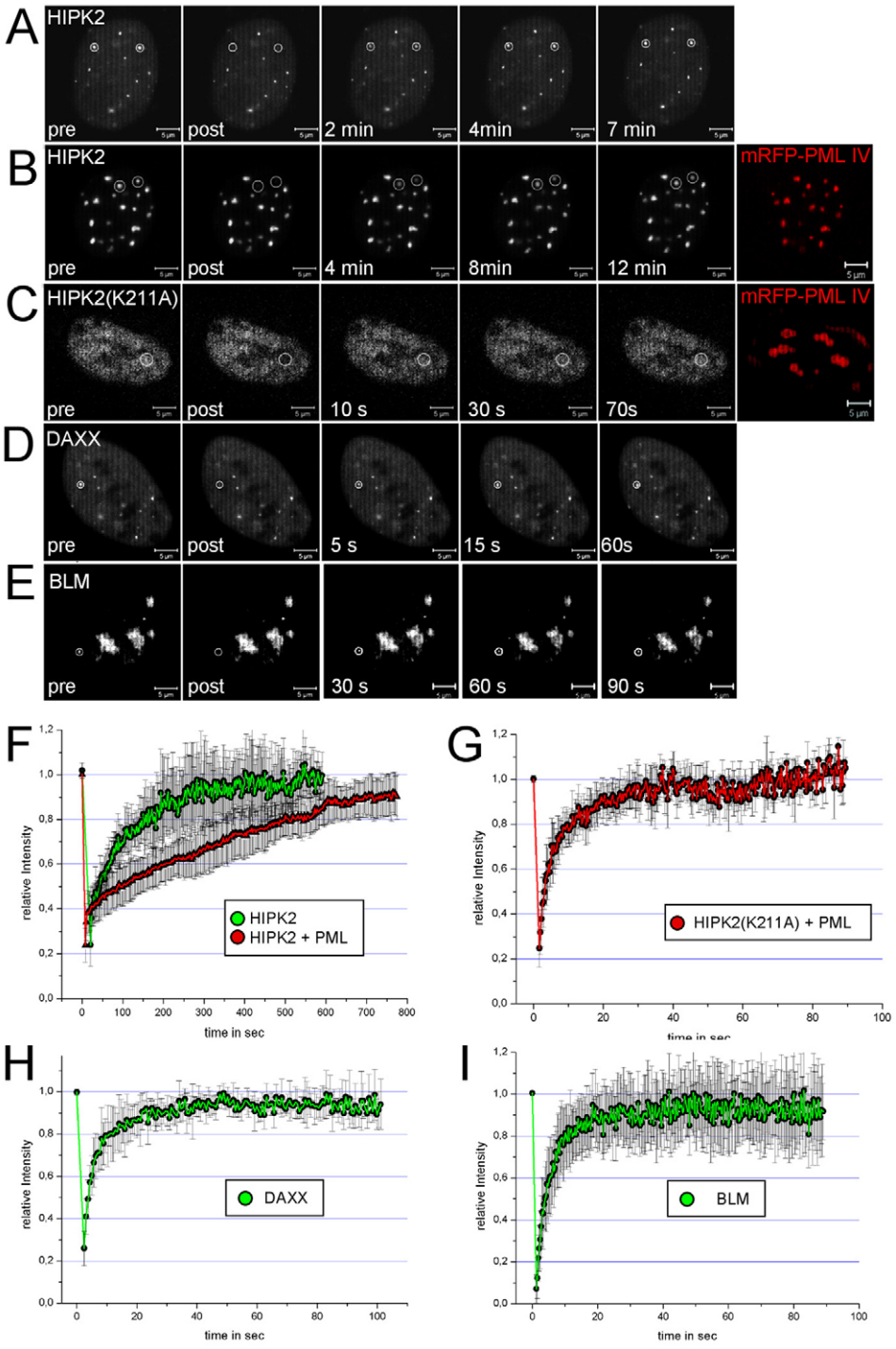

Fig. 7. Exchange dynamics of HIPK2, DAXX and BLM at PML NBs. FRAP experiments were performed in U-2 OS cells that express (A) GFP-tagged wild-type HIPK2, (B) GFP-HIPK2 in combination with mRFP–PML-IV (red), (C) the kinase-defective GFP-HIPK2(K221A) mutant in combination with mRFP–PML-IV (red), GFP-DAXX (D), and GFP-BLM (E). Areas containing HIPK2 accumulations were bleached and fluorescence recovery was recorded for various times as indicated. Scale bars, 5 µm. (F-I) Quantification of FRAP experiments as shown in A-E. Graphs show mean values (± s.d.) from at least 20 FRAP experiments each.

at elevated levels of PML IV. Consistent with previous observations (Hofmann et al., 2002), we observed an enrichment of HIPK2 into PML NBs when mRFP-tagged PML IV was co-expressed (Fig. 7B). Intriguingly, mRFP–PML-IV induced a strong retention of HIPK2 at NBs (Fig. 7F). The recovery halftime of HIPK2 was ~60 seconds in the absence and ~240 seconds in the presence of excess PML IV. These observations clearly indicate that PML IV recruits HIPK2 by increasing its Rt at NBs. We then analyzed GFP-tagged HIPK2(K221A), which lacks the kinase activity (Hofmann et al., 2003). This construct showed only little accumulation at PML NBs, even in the presence of excess mRFP–PML-IV (Fig. 7C, supplementary material Fig. S2D). In addition, the Rt value of HIPK2(K221A) at NBs was only approximately one-fifth of that of wild-type HIPK2 (Table 1). These data demonstrate that a functional kinase domain on HIPK2 is required to retain this enzyme at PML NBs. Interestingly, the diffusion mobility of the kinase mutant throughout the nucleoplasm was reduced fourfold compared with wild-type HIPK2 (Table 1). This observation suggests that the Rt of HIPK2 at nucleoplasmic targets is increased when the kinase is inactive. However, this increased retention in the nucleoplasm is unlikely to contribute significantly to the impaired NB binding of the mutant.

Rapid turnover of DAXX and BLM at PML NBs

We also analyzed exchange kinetics of DAXX and BLM at PML NBs. As reported for exogenous and endogenous DAXX (Ishov et al., 1999), GFP-tagged DAXX localized diffusely in the nucleoplasm and accumulated in SP100-containing PML NBs (supplementary material Fig. S2D). GFP-tagged BLM localized to PML NBs and also in nucleoli in many but not all cells (supplementary material Fig. S2D, and data not shown), in agreement with endogenous BLM distribution in mammalian cells (Sanz et al., 2000). DAXX and BLM showed rapid FRAP at NBs with Rt values of 2.6 seconds and 4.1 seconds, respectively, and the complete pool of NB-bound molecules turned over within less than one minute (Fig. 7H,I). We like to point out that FRAP curves of these proteins could neither be fitted with a binding-diffusion model assuming a single exchanging population (supplementary material Fig. S3N,O), nor with one-component exponential functions (T.L. and P.H., unpublished observations). Therefore, kinetics modeling using the two-component binding-diffusion model reveals at least two

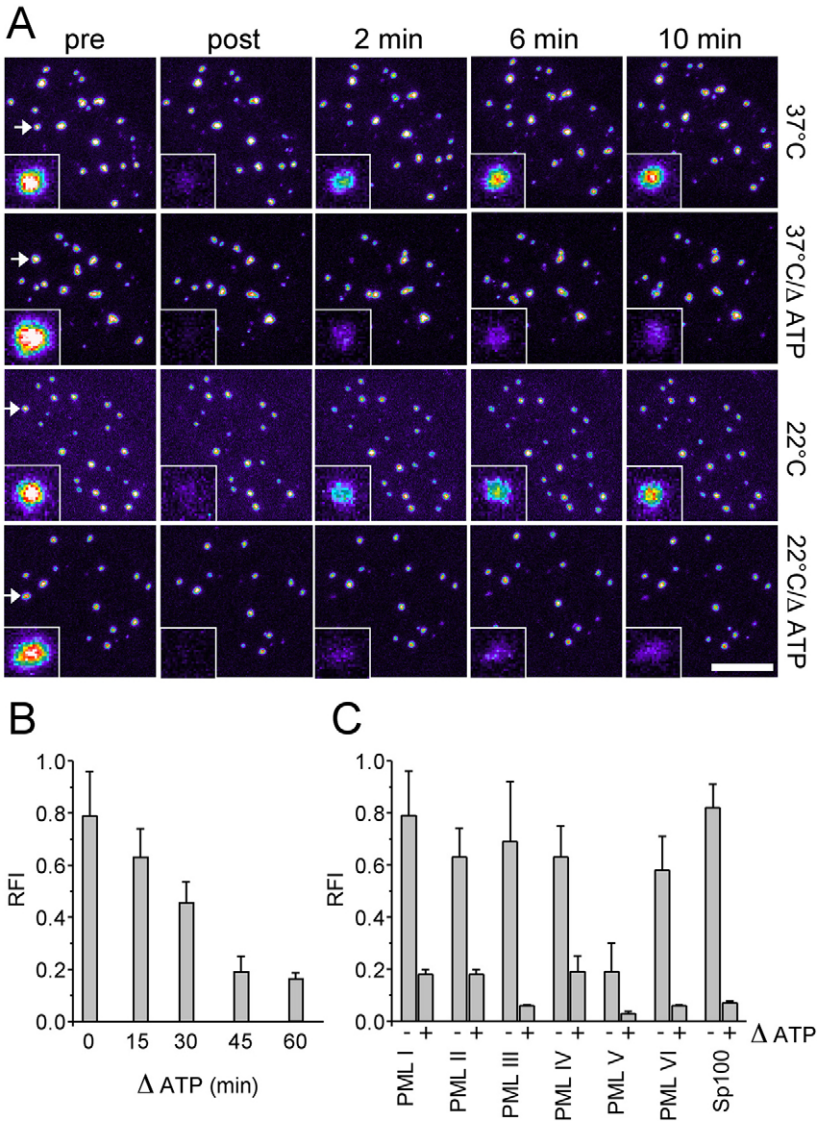

Fig. 8. Protein exchange at PML NBs is dependent on ATP. (A) FRAP experiments were performed on the same GFP–PML-I-expressing U-2 OS cells before (37°C) or after treatment with 10 mM sodium azide/50 mM 2-deoxyglucose for 1 hour (37°C/Δ ATP). Similar experiments were performed at ambient temperature, without or in the presence of ATP-depleting drugs (22°C or 22°C/Δ ATP, respectively). Images represent maximum intensity projections from 3D time-lapse FRAP data sets. Arrows indicate bleached regions that contain a PML NB; these areas are also shown as enlarged insets. Scale bar, 5 μm. (B) FRAP experiments as described in A were performed on cells after the indicated times of ATP depletion. Fluorescence recovery after 10 minutes of the bleach pulse was quantified from 30 PML NBs (3 NBs ×10 cells each) and displayed as mean ± s.d. (C) FRAP experiments as described in A were performed on cells that express the indicated GFP fusion protein after 60 minutes of ATP depletion. Fluorescence recovery at NBs after 10 minutes of the bleach pulse was quantified from ten cells each and displayed as the mean ± s.d.

differently mobile populations of DAXX and BLM at PML NBs, a fast one that rapidly binds and unbinds at the surface, and a slower one that is retained at NBs within seconds. The mayority (>80%) of GFP-tagged DAXX or BLM molecules was identified in the more loosely bound fraction by kinetics modeling (Table 1). Outside NBs, both proteins move by anomalous diffusion indicating transient binding events of DAXX and BLM at less mobile interaction sites throughout the nuclear volume (Table 1).

ATP levels but not temperature affect component exchange at PML NBs

We next depleted ATP levels in U-2 OS cells that were transfected with GFP–PML-I. Treatment of cells with the respiration inhibitor sodium azide in conjunction with the glycolysis inhibitor 2-deoxyglucose caused no detectable change in size or morphology of PML NBs (Fig. 8A). Depletion of cellular ATP levels induced a strong decrease of GFP–PML-I exchange at NBs. By contrast, lowering the incubation temperature from 37°C to 22°C had no effect (Fig. 8A). NB immobilization of GFP–PML-I in ATP-depleted cells decreased linearly as a function of drug incubation time and reached a plateau after 45 minutes (Fig. 8B). By contrast, mobility of GFP–PML-I outside NBs was unaffected during ATP depletion (supplementary material Fig. S4A,B). Recovery of cells for 1 hour after drug washout restored fluorescence recovery of GFP–PML-I at NBs, revealing that the ATP-depletion effect on GFP–PML-I exchange is reversible when ATP synthesis is reinitiated (supplementary material Fig. S4C,D). ATP-dependent immobilization was not specific for PML I because all other PML isoforms and SP100 showed the same behavior (Fig. 8C). On the basis of these observations we conclude that component exchange at PML NBs is purely diffusion-driven but that ATP homeostasis appears to be crucial for the association dynamics.

Discussion

Understanding PML NB assembly and function requires detailed knowledge of its organization in space and time. Using live-cell microscopy and kinetics modeling we have determined the intranuclear dynamics of eleven components of PML NBs. These data reveal a wide range of assembly plasticity of PML NBs (Fig. 9).

PML traffic at NBs

Previous analyses on component exchange at PML NBs had used only the isoform PML IV in FRAP experiments (Boisvert et al., 2001; Wiesmeijer et al., 2002; Everett et al., 2005). In the present study we have analyzed all six nuclear PML isoforms by FRAP and FCS. The GFP-tagged isoforms showed protein-specific exchange dynamics at NBs. The sequence of the shortest isoform, PML VI, is shared by all others and, hence, the nuclear dynamics associated with PML VI may be considered to be inherent to all other isoforms. We had therefore expected that PML VI has the longest Rt at NBs. Indeed, compared with PML isoforms I to IV this is true. PML VI does not contain the SUMO-interacting motif, however, its exchange is only marginally slower than isoforms I to IV, all of which contain a SIM. This indicates that the SIM domain, although probably necessary for de novo formation of NBs (Shen et al., 2006), is not a main regulator of PML turnover dynamics at NBs. The high exchange rates of PML isoforms I to IV are most likely to reflect the existence of diverse functional domains at their C-termini as,

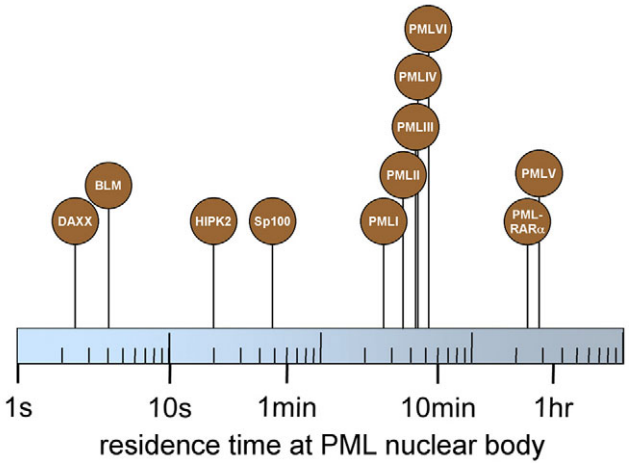

Fig. 9. Dynamics of component exchange at PML NBs. The Rt values of the indicated PML NB components as deduced from our kinetics-modeling approach is shown on a logarithmic seconds scale.

for example, in the case of PML I (Condemine et al., 2007). Indeed, PML isoforms have been shown to associate differentially with certain proteins (Fogal et al., 2000). Freely diffusing PML isoforms might bind to interaction partners for efficient NB targeting of these factors for downstream events such as sequestration, complex assembly, post-translational modifications or proteolytic degradation. We suggest that the NB 'provides' six nuclear PML isoforms with individual binding surfaces that 'scan' the nucleoplasm for potential interaction partners. Scanning by PML proteins requires overall availability through high mobility, and short interactions, which is exactly what we determined by FCS. A functional interaction between scanning PML isoforms and specific binding factors outside NBs might also serve to seed new ones, i.e. at invading viral DNA (Everett and Murray, 2005) or at single- or double-strand DNA breaks (Carbone at al., 2002; Bøe et al., 2006). Alternatively, nuclear proteins might retrieve specific PML isoforms from the NB through specific interactions. The complexes might then act together on nearby chromatin as, for example, suggested for the SATB1/PML interaction network that regulates expression of MHC class I genes (Kumar et al., 2007). These scenarios are not mutually exclusive and are likely to contribute to the individual binding times of PML isoforms at NBs.

PML V as a scaffold subunit of NBs?

It came as a surprise that PML V is a very stable isoform at NBs. Kinetics modeling revealed an Rt value of 48 minutes, and 80% exchange is reached only after more than 2 hours (Table 1, and our unpublished data). By contrast, typical Rt values of proteins within speckles, Cajal bodies (CB) and nucleoli range between seconds to a few minutes (Phair and Misteli 2000; Kruhlak et al., 2000; Chen and Huang, 2001; Handwerger et al., 2003; Dundr et al., 2004). The fast exchange reflects rapid association/dissociation cycles of the components between the NB and the nucleoplasm, similar to speckles, Cajal bodies and nucleoli (Misteli, 2008). This model is compatible with the data we obtained for all PML NB components, except PML V. Its high Rt value and extremely low off-rate (k_{off} =4×10^{-4} second^{-1}) at NBs is unlikely to reflect involvement in a biochemical reaction but rather is indicative of a structural role of this isoform within PML NBs. Kinetics modeling also revealed tightly bound populations (k_{in}/k_{out}) of the other PML isoforms (Table 1). We therefore propose that subpopulations of all PML isoforms in a NB can be part of a three-dimensional meshwork structure of hetero-oligomerized PML isoforms (Kentsis et al., 2002) where PML V serves as a long-lasting but not static scaffold subunit. Such a metastable PML scaffold has the advantage to be able to rapidly respond to external stimuli, while at the same time serving as a stable platform for the assembly of functional complexes built from faster-exchanging molecules, such as DAXX, BLM, HIPK2 and CBP, with Rt values of several seconds (Table 1) (Everett and Murray, 2005; Boisvert et al., 2001). Building such complexes at the 'catalytic surface' of a NB might promote specificity and speed. Indeed, other RING-containing protein domains exhibit polyvalent scaffolding as a result of self-assembly to control of their specific biochemical activities (Kentsis et al., 2002). Supramolecular self-assembly equips living cells with the genetic economy of forming large meso- and macroscopic

Table 1. Dynamics of PML NB components in the nucleoplasm and at NBs

Protein	D [μm^2 second^{-1}]	α	k_{on} [second^{-1}]	k_{off} [second^{-1}]	k_{in} [second^{-1}]	k_{out} [second^{-1}]	Rt [second]	bnd$_{out}$	bnd$_{in}$
PML I	1.85	0.47	0.0698	0.0051	0.0017	0.0045	272.3	0.7216	0.2784
PML II	1.03	0.44	0.0510	0.0051	0.0013	0.0015	372.7	0.5263	0.4737
PML III	1.63	0.53	0.0421	0.0026	<0.0001	<0.0001	450.9	0.8663	0.1337
PML IV	1.04	0.50	0.0420	0.0034	0.0007	0.0012	452.9	0.6416	0.3584
PML V	2.79	0.57	0.0065	0.0004	<0.0001	<0.0001	2900.9	0.7232	0.2768
PML VI	1.49	0.51	0.0358	0.0027	<0.0001	<0.0001	530.6	0.6981	0.3019
PML IV-2K	1.19	0.55	0.0860	0.2709	0.0118	0.0205	5.8	0.6348	0.3651
PML IV-3K	2.23	0.61	0.0657	0.0293	0.0046	0.0001	1507.1	0.0227	0.9773
PML-RARα	0.93	0.45	0.0039	0.0018	0.0024	0.0070	2297.0	0.2413	0.7587
SP100	1.23	0.62	0.3940	0.0578	0.0103	0.0058	48.2	0.3585	0.6415
SP100K297R	0.84	0.58	0.8517	0.0978	0.0003	0.0003	22.3	0.4585	0.5415
HIPK2	2.60	0.66	0.2722	0.6216	0.0744	0.0127	11.0	0.8540	0.1460
HIPK2mut	0.66	0.50	0.4242	0.8173	0.0730	0.0788	2.4	0.5190	0.4810
DAXX	0.95	0.60	0.7552	0.4683	0.0028	0.0116	2.6	0.8064	0.1936
BLM	3.10	0.61	0.9700	0.2765	0.0009	0.0062	4.1	0.8769	0.1231
nls-GFP	9.50	0.73	n.a.	n.a.	n.a.	n.a.	n.a.	n.a.	n.a.

The diffusion-binding model was used to extract kinetics data from the FRAP experiments of the indicated PML NB components after fitting. The diffusion coefficients (D) and the anomaly parameters (α) were determined by FCS. k_{on}, association rate at the surface of the nuclear body; k_{off}, dissociation rate at the surface of the nuclear body; k_{in}, penetration rate into the nuclear body; k_{out}, penetration rate out of the core of the nuclear body; Rt, mean residence time at nuclear bodies; bnd$_{out}$, fraction of molecules residing at the surface of the nuclear body; bnd$_{in}$, fraction of molecules residing in the core of the nuclear body. FCS data obtained for GFP tagged with a nuclear localization signal (nls-GFP) are also shown (n.a., not applicable).

structures, while minimizing the use of genetic material (Kentsis and Borden, 2004). Obviously, alternative splicing of the PML mRNA transcript evolved as an additional mechanism to oppose this genetic restriction in order to supply both structural stability and functional flexibility (Fig. 9). A meta-stable scaffold organization of PML NBs might also grant sustained chromatin contacts (Eskiw et al., 2004), providing the biophysical requirements for the positional stability of PML NBs in chromatin (Wiesmeijer et al., 2002; Görisch et al., 2004), at damaged DNA sites over hours (Dellaire and Bazett-Jones, 2004), at viral genomes (Everett, 2006) or at the MHC gene cluster (Shiels et al., 2001; Kumar et al., 2007).

Targeting and release mechanisms at PML NBs

Altering the PML isoform content of PML NBs might not only affect the proteins recruited to these bodies, but might also modulate their nuclear positioning and functional interaction with chromatin (Kumar et al., 2007). Our data highlight possible mechanisms by which the dynamics of component exchange at PML NBs can be modulated.

As already discussed in detail, differential expression of PML isoforms might directly modulate exchange kinetics of both PML and PML-interacting proteins. We also showed that the SUMOylation pattern dictates Rt values of PML at NBs. At low expression levels, GFP–PML–SUMO-3K localized to normal NBs but its exchange was extremely slow. Thus, complete de-SUMOylation is not only a means to partially disassemble PML NBs at mitosis (Sternsdorf et al., 1997; Everett et al., 1999) but also to render PML molecules immobile (Fig. 5H), as evidenced by mitotic accumulations of PML protein (MAPPs) in living mitotic cells (Dellaire et al., 2006). By contrast, PML–SUMO-2K was hypermobile at NBs (Fig. 5G), revealing that Lys65 SUMOylation is required for increased NB retention of PML. The three SUMOylation sites on PML provide a considerable number of combinatorial modifications that might translate into distinct Rt values at NBs. That SUMO modification is a tool to fine-regulate the dynamics of a protein at NBs was also observed for de-SUMOylated SP100 (Fig. 6), which showed wild-type-like binding at the NB surface (k_{on}/k_{off}), but increased retention in the core (k_{in}/k_{out}; Table 1). Reduction of the cellular ATP level induced an immobilization of all PML isoforms and also SP100 at NBs. Since, however, component exchange was unaltered in cells grown at 22°C (Fig. 8A), an energy-dependent mechano-chemical remodeling activity is unlikely to contribute to exchange dynamics at PML NBs. We rather suggest that ATP depletion decreases the phosphorylation status of PML molecules, which in turn might lead to their immobilization at NBs. Indeed, PML is phosphorylated at several residues by specific kinases, and these modifications modulate apoptotic and tumor-suppressive properties of PMLs (Bernardi and Pandolfi, 2007). Whatever the molecular mechanism, the cellular ATP level appears to be yet another crucial switch in controlling the release of factors from PML NBs. Finally, regulated expression of one isoform might alter the exchange rate of other components, as we demonstrated for PML–SUMO-2K, PML IV or HIPK2, all of which become less mobile upon coexpression of wild-type PML IV, PML-RARα or PML IV, respectively.

In conclusion, the time a component stays at PML NBs might be modulated by (1) its own SUMOylation status, (2) the presence of a SIM (Lin et al., 2007), (3) the PML isoform it binds to, (4) the SUMOylation pattern of this isoform, (5) the cellular ATP level and, (6) the relative abundance of other isoforms in the same NB. Different SUMO paralogs, polymeric SUMO chains and phosphorylation could provide additional layers.

PML-RARα is suggested to interfere with normal myeloid differentiation by inhibiting wild-type RARα transcriptional activity (Melnick and Licht, 1999). On the basis of FRAP analyses it has recently been proposed that PML-RARα expression interferes with normal RARα functions by reducing the intranuclear mobility of RARα and its co-regulator SMRT, suggesting a crucial role for the reduced intranuclear mobility of PML-RARa in the pathogenesis of APL (Dong et al., 2004; Huang et al., 2007). Here, we demonstrated that the PML-RARα oncogene can efficiently immobilize wild-type PML proteins. It is therefore possible that the amount of available wild-type PML in the nucleoplasm is drastically reduced through increased hetero-oligomerization with PML-RARα. However, whether this PML-RARα-induced immobilization of wild-type PML isoforms contributes to a block of monocyte differentiation and APL pathogenesis remains to be tested.

PML NBs: active or passive nuclear sites?

Several models have been proposed to explain PML NB function. These domains might operate (1) as nuclear storage sites for the accumulation or sequestration of proteins, (2) as catalytic surfaces where proteins accumulate to be post-translationally modified, or (3) as active sites for specific nuclear functions such as transcriptional and chromatin regulation (reviewed in Bernardi and Pandolfi, 2007). During a stress response, HIPK2-mediated phosphorylation of p53 and acetylation by CBP is believed to occur at PML NBs (Guo et al., 2000; Fogal et al., 2000; Hofmann et al., 2002; D'Orazi et al., 2002). Here, we have shown that, even in the presence of excess PML IV, HIPK2 binding to NBs was almost absent when its kinase is inactive. Furthermore, quantitative expression of PML IV increased the Rt of wild-type HIPK2 at NBs several fold. These observations strengthen the catalytic-platform theory for PML NBs, which suggests that specific processes (phosphorylation, acetylation, SUMOylation), occur on the surface of the body (Kentsis and Borden, 2004). Support for such a scenario comes from recent in situ analyses that indicate that SUMOylation or proteasomal protein degradation occur at a subset of PML NBs (Lallemand-Breitenbach, 2001; Rockel et al., 2005; Saitoh et al., 2006), and from the observation that PML itself might act as a SUMO ligase (Quimby et al., 2006). BLM and DAXX turned over at NBs rapidly and completely. Since these proteins function directly at DNA-synthesis sites or at specific promoters, respectively (Wu, 2007; Lin et al., 2007), their low Rt values are likely to reflect the function of PML NBs to titrate the concentration of these factors in the nucleus. Intriguingly, more than 80% of BLM and DAXX molecules at NBs belonged to the more-loosely bound population, as revealed by our kinetics-modeling approach (bnd_{out}; Table 1). SP100 is also a transcriptional co-regulator at promoters but showed dissociation kinetics that were one order of magnitude slower at PML NBs than those of BLM or DAXX. Although this does not rule out a titration effect by NBs, the Rt value for SP100 also suggests a scaffold function for the regulated retention of SP100-interacting proteins at NBs, such as NBS1 and HP1 (Naka et al., 2002; Seeler et al., 1998). Our kinetics data do not favor a particular model for PML NB function but, instead, provide evidence for all of them. We therefore suggest that PML NBs are integrated into many nuclear pathways as both biophysical and biochemical hubs, which provide at the same time structural stability at specific chromatin loci, titration sites for specific factors as well as catalytic surfaces for post-translational modifications or complex assembly.

Material and Methods

Plasmids

GFP-expression constructs are described in supplementary material Table S1.

Cell culture and transfection

U-2 OS, HEp-2, and HeLa cells obtained from the American Tissue Culture Collection (ATCC) were cultured in Dulbecco's modified Eagle's medium (DMEM) supplemented with 10% fetal calf serum in a 10% CO_2 atmosphere at 37°C. For live cell imaging experiments, cells were seeded on 42-mm glass dishes (Saur Laborbedarf, Reutlingen, Germany) and, 1-2 days before observation, transfected with plasmid DNA by using FuGENE-HD Transfection reagent (Roche, Basel, Switzerland) according to the manufacturer's protocol. Stable cell lines were seeded similarly without transfection. ATP depletion was induced by 10 mM sodium azide/50 mM 2-deoxyglucose (Sigma, Deisenhofen, Germany) final concentration in the cell culture medium, as described previously (Platani et al., 2002). In ATP-recovery experiments the ATP depletion media was replaced by normal media for 1hr.

Western blots

Whole-cell extracts were produced from transiently or stably transfected cell lines, separated by SDS-PAGE and transferred to the Protran nitrocellulose membrane (Schleicher & Schuell, Dassel, Germany). The membrane was incubated with primary antibodies (in PBS-T) and developed with a peroxidase-conjugated species-specific secondary antibodies (Jackson ImmunoResearch, West Grove, PA). Signals were detected using the ECL reagent (Amersham, Uppsala, Sweden) on imaging film (Biomax, Kodak, Stuttgart, Germany). Anti-GFP monoclonal antibody was from Santa-Cruz Biotechnology (Heidelberg, Germany), anti-PML rabbit antibody (ABD-030) from Jena Biosciences (Germany), and anti-tubulin monoclonal antibody from Sigma (Germany).

Immunocytochemistry and microscopy

Cells grown on 15-mm diameter coverslips were fixed with 4% formaldehyde for 10 minutes and permeabilized with 0.25% Triton X-100 for 3 minutes. Rabbit anti-PML (ABD-030, Jena Biosciences, Germany) and anti-SP100 antibodies (ABD-031, Jena Biosciences) were incubated with cells for 45 minutes. After washing steps with PBS, anti-rabbit secondary antibody coupled to Cy3 (Jackson ImmunoResearch, PA) was incubated with cells for 45 minutes, followed by a DNA-staining step by using ToPro3 (Invitrogen, Carlsbad, CA) for 10 minutes and mounting with Prolong Gold antifade mounting medium (Invitrogen). For microscopy, a LSM 510Meta laser scanning confocal microscope (Carl Zeiss, Jena, Germany) was used as previously described (Weidtkamp-Peters et al., 2008).

Fluorescence correlation spectroscopy measurements

Fluorescence correlation spectroscopy (FCS) measurements were performed at 37°C on a LSM 510Meta/ConfoCor2 combi system using a C-Apochromat infinity-corrected 1.2 NA 40× water objective (Carl Zeiss, Jena, Germany) as described in detail elsewhere (Schmiedeberg et al., 2004; Weidtkamp-Peters et al., 2008). Briefly, GFP-tagged proteins were spot-illuminated with the 488 nm line of a 20 mW Argon laser at 5.5 A tube current attenuated by an acousto-optical tunable filter (AOTF) to 0.1%. The detection pinhole had a diameter of 70 µm and emission was recorded through a 505-nm long-path filter. For the measurements, 10×30 time series of 10 seconds each were recorded with a time resolution of 1 µsecond and then superimposed for fitting to an anomalous diffusion model in three dimensions with triplet function (Saxton, 2001) using Origin Software (OriginLab, Northhampton, MA). The *D* values and anomaly parameters were extracted from fit curves as previously described (Hemmerich et al., 2008).

Fluorescence recovery after photobleaching

Fluorescence recovery after photobleaching (FRAP) experiments were carried out on a Zeiss LSM 510Meta confocal microscope (Carl Zeiss, Jena, Germany) essentially as described before (Hemmerich et al., 2008). Five to ten images were taken before the bleach pulse and 50-200 images after the bleaching of regions of interest (ROIs) that contained one NB each at 0.05% laser transmission to minimize scan bleaching. Image-acquisition frequency was adapted to the recovery rate of the respective GFP-fusion protein. The pinhole was adjusted to 1 airy unit. Quantification of relative fluorescence intensities was done according to Schmiedeberg et al. (Schmiedeberg et al., 2004) using Excel (Microsoft, Redmond, WA) and Origin software (OriginLab, Northhampton, MA).

Reaction-diffusion model

For the mathematical model, the structural complexity of a PML body has been estimated assuming that molecules that undergo binding and unbinding to and from the body do so at the surface, and molecules situated more towards the inside of the body cannot unbind before moving to the surface. There is thus a reservoir of tightly bound 'inner' molecules and one of loosely bound 'outer' ones. Exchange between these reservoirs is modeled by linear kinetics, i.e. the more molecules there are, the more will move inside or out with rate constants k_{in} and k_{out}, respectively. Binding and unbinding to the PML body is treated similarly, with rate constants k_{in} and k_{out}, respectively. The experimental set-up provided that bleached ROI and FRAP ROI are similar and, so, are assumed to be the same for modeling purposes. Diffusion inside and out of the ROI was modeled as a linear two-way process with a rate constant of $2D/r$, where the D value was measured by FCS, and r is the radius of the ROI. This constant yields the effective exchange rate through the boundary of a circular area. The model considers only fluorescent molecules of one type at a time, so no interactions between different molecular species are considered. It distinguishes between molecules outside the ROI, inside the ROI but diffusing freely, loosely bound at the surface of the PML body, and tightly bound inside the body. The fluorescence outside the ROI is all but unchanged by the bleaching pulse and subsequent diffusion, so all fluorescence values in the model were divided by this value, resulting in a normalized fluorescence scale that is the same across the different molecular species. Describing normalized concentrations of the fluorescent protein in free diffusion (x), loosely bound (y) and tightly bound (z), the reaction system results in the model equations

$$\frac{dx}{dt} = k_{off}\,y - k_{on}x + \frac{2D}{r}(1-x)$$
$$\frac{dy}{dt} = k_{on}x - k_{off}\,y + k_{out}z - k_{in}y$$
$$\frac{dz}{dt} = k_{in}y - k_{out}z\,.$$

For each type of observed molecule, we determined the ratio p of steady-state fluorescence in the background and in the body (see below), which enabled us to express the observable fluorescence in the ROI as

$$w(t) = \frac{x(t) + y(t) + z(t)}{p}\,.$$

Since the amount of bleached molecules is small compared with the overall amount of molecules in the nucleus, it is plausible to assume that, after a sufficiently long time, fluorescence returns to the value measured before photobleaching. This constraint removes one degree of freedom from the model, yielding

$$k_m = \frac{1-p}{p} \times \frac{k_{off}}{1 + k_m / k_{out}}\,.$$

The differential equations were numerically solved using an explicit Runge-Kutta formula (method ode45 in MATLAB). To fit the parameters of the model, an evolution strategy with covariance matrix adaptation (CMA-ES) was employed (Hansen and Ostermeier 2001).

The ratio between background fluorescence and fluorescence inside the PML-body (p) was determined individually for each type of molecule by using confocal microscopy, and pixel intensity evaluation by using MetaMorph software (Molecular Devices, Sunnyvale, CA). The following p values were obtained for the GFP fusion proteins: all PML isoforms, p=20; PML-RARα, p=10; all SP100 constructs, p=20; DAXX, p=3; HIPK2, p=2; HIPK2(K221A), p=2; PML–SUMO-2K, p=1.5; PML–SUMO-3K, p=100, BLM, p= 5. These values were used to normalize the concentrations used in the model. The mathematical model treats normalized concentrations of fluorescent molecules in free diffusion (x), loosely bound (y) and tightly bound (z) to the PML body.

It is important to note that the concentration values x, y and z have been normalized to the background fluorescence outside the region of interest. Since we have determined the ratio p between equilibrium fluorescence inside the body and outside the ROI, and because the data used to fit the model were given in relative fluorescence intensity with an equilibrium value of 1, the background fluorescence is given as $1/p$. Therefore, the observed RFI value w is related to the model concentrations by

$$w(t) = \frac{x(t) + y(t) + z(t)}{p}\,.$$

Over a very long time, all molecular species in the PML-body will eventually turn over, so that it is reasonable to assume $w(t)$ tends towards 1 for a large t value. This means that for equilibrium conditions, in which

$$\frac{dx}{dt} = \frac{dy}{dt} = \frac{dz}{dt} = 0$$

we get $w(t)$=1. In this case, we have

$$k_{in}y - k_{out}z = 0$$
$$k_{on}x - k_{off}\,y + k_{out}z - k_{in}y = 0$$
$$k_{off}\,y - k_{on}x + \frac{2D}{r}(1-x) = 0$$
$$x + y + z = p$$

and, thus, from the first three lines, we get

$$z = \frac{k_{in}}{k_{out}} y$$

$$y = \frac{k_{on}}{k_{off}} x$$

$$x = 1.$$

Finally, taking this together with the condition $x + y + z = p$, we find

$$1 + \frac{k_{on}}{k_{off}} + \frac{k_{in}k_{on}}{k_{out}k_{off}} = p$$

$$\Rightarrow k_{on} = \frac{k_{off}(p-1)}{1 + k_{in} / k_{out}}$$

which enabled us to remove one degree of freedom k_{on} from the model.

We thank S. Ohndorf and M. Koch for technical assistance. We are grateful to K. S. Chang, N. Ellis, S. Dong and T. Yeh for the kind gift of plasmids. P.H. thanks Stephan Diekmann for enlightning discussions. T.L. thanks Bashar Ibrahim for fruitful discussions and the EU (ESIGNET, project no. 12789) for financial support. This work was supported by grant HE 2484/3-1 from the Deutsche Forschungsgemeinschaft.

References

Ascoli, C. A. and Maul, G. G. (1991). Identification of a novel nuclear domain. *J. Cell Biol.* **112**, 785-795.

Banks, D. S. and Fradlin, C. (2005). Anomalous diffusion of proteins due to molecular crowding. *Biophys. J.* **89**, 2960-2971.

Bernardi, R. and Pandolfi, P. P. (2007). Structure, dynamics and functions of promyelocytic leukaemia nuclear bodies. *Nat. Rev. Mol. Cell. Biol.* **8**, 1006-1016.

Bøe, S. O., Haave, M., Jul-Larsen, A., Grudic, A., Bjerkvig, R. and Lønning, P. E. (2006). Promyelocytic leukemia nuclear bodies are predetermined processing sites for damaged DNA. *J. Cell Sci.* **119**, 3284-3295.

Boisvert, F. M., Hendzel, M. J. and Bazett-Jones, D. P. (2000). Promyelocytic leukemia (PML) nuclear bodies are protein structures that do not accumulate RNA. *J. Cell Biol.* **148**, 282-292.

Boisvert, F. M., Kruhlak, M. J., Box, A. K., Hendzel, M. J. and Bazett-Jones, D. P. (2001). The transcription coactivator CBP is a dynamic component of the promyelocytic leukemia nuclear body. *J. Cell Biol.* **152**, 1099-1106.

Borden, K. L. (2002). Pondering the promyelocytic leukemia protein (PML) puzzle: possible functions for PML nuclear bodies. *Mol. Cell. Biol.* **22**, 5259-5269.

Carbone, R., Pearson, M., Minucci, S. and Pelicci, P. G. (2002). PML NBs associate with the hMre11 complex and p53 at sites of irradiation induced DNA damage. *Oncogene* **21**, 1633-1640.

Chen, D. and Huang, S. (2001). Nucleolar components involved in ribosome biogenesis cycle between the nucleolus and nucleoplasm in interphase cells. *J. Cell Biol.* **153**, 169-176.

Condemine, W., Takahashi, Y., Zhu, J., Puvion-Dutilleul, F., Guegan, S., Janin, A. and de The, H. (2006). Characterization of endogenous human promyelocytic leukemia isoforms. *Cancer Res.* **66**, 6192-6198.

Condemine, W., Takahashi, Y., Le Bras, M. and de Thé, H. (2007). A nucleolar targeting signal in PML-I addresses PML to nucleolar caps in stressed or senescent cells. *J. Cell Sci.* **120**, 3219-3227.

D'Orazi, G., Cecchinelli, B., Bruno, T., Manni, I., Higashimoto, Y., Saito, S., Gostissa, M., Coen, S., Marchetti, A., Del Sal, G. et al. (2002). Homeodomain-interacting protein kinase-2 phosphorylates p53 at Ser 46 and mediates apoptosis. *Nat. Cell Biol.* **4**, 11-19.

Daniel, M. T., Koken, M., Romagné, O., Barbey, S., Bazarbachi, A., Stadler, M., Guillemin, M. C., Degos, L., Chomienne, C. and de Thé, H. (1993). PML protein expression in hematopoietic and acute promyelocytic leukemia cells. *Blood* **82**, 1858-1867.

Dellaire, G. and Bazett-Jones, D. P. (2004). PML nuclear bodies: dynamic sensors of DNA damage and cellular stress. *Bioessays* **26**, 963-977.

Dellaire, G., Eskiw, C. H., Dehghani, H., Ching, R. W. and Bazett-Jones, D. P. (2006). Mitotic accumulations of PML protein contribute to the re-establishment of PML nuclear bodies in G1. *J. Cell Sci.* **119**, 1034-1042.

de Thé, H., Chomienne, C., Lanotte, M., Degos, L. and Dejean, A. (1990). The t(15;17) translocation of acute promyelocytic leukaemia fuses the retinoic acid receptor alpha gene to a novel transcribed locus. *Nature* **347**, 558-561.

Dong, S., Stenoien, D. L., Qiu, J., Mancini, M. A. and Tweardy, D. J. (2004). Reduced intranuclear mobility of APL fusion proteins accompanies their mislocalization and results in sequestration and decreased mobility of retinoid X receptor alpha. *Mol. Cell. Biol.* **24**, 4465-4475.

Dundr, M., Hebert, M. D., Karpova, T. S., Stanek, D., Xu, H., Shpargel, K. B., Meier, U. T., Neugebauer, K. M., Matera, A. G. and Misteli, T. (2004). In vivo kinetics of Cajal body components. *J. Cell Biol.* **164**, 831-842.

Dyck, J. A., Maul, G. G., Miller, Jr, W. H., Chen, J. D., Kakizuka, A. and Evans, R. M. (1994). A novel macromolecular structure is a target of the promyelocyte-retinoic acid receptor oncoprotein. *Cell* **76**, 333-343.

Eskiw, C. H., Dellaire, G. and Bazett-Jones, D. P. (2004). Chromatin contributes to structural integrity of promyelocytic leukemia bodies through a SUMO-1-independent mechanism. *J. Biol. Chem.* **279**, 9577-9585.

Everett, R. D. (2006). Interactions between DNA viruses, ND10 and the DNA damage response. *Cell. Microbiol.* **8**, 365-374.

Everett, R. D. and Murray, J. (2005). ND10 components relocate to sites associated with herpes simplex virus type 1 nucleoprotein complexes during virus infection. *J. Virol.* **79**, 5078-5089.

Everett, R. D., Lomonte, P., Sternsdorf, T., van Driel, R. and Orr, A. (1999). Cell cycle regulation of PML modification and ND10 composition. *J. Cell Sci.* **112**, 4581-4588.

Fogal, V., Gostissa, M., Sandy, P., Zacchi, P., Sternsdorf, T., Jensen, K., Pandolfi, P. P., Will, H., Schneider, C. and Del Sal, G. (2000). Regulation of p53 activity in nuclear bodies by a specific PML isoform. *EMBO J.* **19**, 6185-6195.

Gambacorta, M., Flenghi, L., Fagioli, M., Pileri, S., Leoncini, L., Bigerna, B., Pacini, R., Tanci, L. N., Pasqualucci, L., Ascani, S. et al. (1996). Heterogeneous nuclear expression of the promyelocytic leukemia (PML) protein in normal and neoplastic human tissues. *Am. J. Pathol.* **149**, 2023-2035.

Goddard, A. D., Borrow, J., Freemont, P. S. and Solomon, E. (1991). Characterization of a zinc finger gene disrupted by the t(15;17) in acute promyelocytic leukemia. *Science* **254**, 1371-1374.

Görisch, S. M., Wachsmuth, M., Ittrich, C., Bacher, C. P., Rippe, K. and Lichter, P. (2004). Nuclear body movement is determined by chromatin accessibility and dynamics. *Proc. Natl. Acad. Sci. USA* **101**, 13221-13226.

Guo, A., Salomoni, P., Luo, J., Shih, A., Zhong, S., Gu, W. and Pandolfi, P. P. (2000). The function of PML in p53-dependent apoptosis. *Nat. Cell Biol.* **2**, 730-736.

Handwerger, K. E., Murphy, C. and Gall, J. G. (2003). Steady-state dynamics of Cajal body components in the Xenopus germinal vesicle. *J. Cell Biol.* **160**, 495-504.

Hansen, N. and Ostermeier, A. (2001). Completely derandomized self-adaptation in evolution strategies. *Evolutionary Computation* **9**, 159-195.

Hemmerich, P. and Diekmann, S. (ed.) (2005). *Visions of the Cell Nucleus*. CA, USA: American Scientific Publishers.

Hemmerich, P., Weidtkamp-Peters, S., Hoischen, C., Schmiedeberg, L., Erliandri, I. and Diekmann, S. (2008). Dynamics of inner kinetochore assembly and maintenance in living cells. *J. Cell Biol.* **180**, 1101-1114.

Hink, M. A., Griep, R. A., Borst, J. W., van Hoek, A., Eppink, M. H., Schots, A. and Visser, A. J. (2000). Structural dynamics of green fluorescent protein alone and fused with a single chain Fv protein. *J. Biol. Chem.* **275**, 17556-17560.

Hofmann, T. G., Moller, A., Sirma, H., Zentgraf, H., Taya, Y., Droge, W., Will, H. and Schmitz, M. L. (2002). Regulation of p53 activity by its interaction with homeodomain-interacting protein kinase-2. *Nat. Cell Biol.* **4**, 1-10.

Hofmann, T. G., Stollberg, N., Schmitz, M. L. and Will, H. (2003). HIPK2 regulates transforming growth factor-beta-induced c-Jun NH(2)-terminal kinase activation and apoptosis in human hepatoma cells. *Cancer Res.* **63**, 8271-8277.

Huang, Y., Qiu, J., Chen, G. and Dong, S. (2007). Coiled-coil domain of PML is essential for the aberrant dynamics of PML-RARalpha, resulting in sequestration and decreased mobility of SMRT. *Biochem. Biophys. Res Commun.* **365**, 258-265.

Ishov, A. M., Sotnikov, A. G., Negorev, D., Vladimirova, O. V., Neff, N., Kamitani, T., Yeh, E. T., Strauss, J. F. R. and Maul, G. G. (1999). PML is critical for ND10 formation and recruits the PML-interacting protein daxx to this nuclear structure when modified by SUMO-1. *J. Cell Biol.* **147**, 221-234.

Jensen, K., Shiels, C. and Freemont, P. S. (2001). PML protein isoforms and the RBCC/TRIM motif. *Oncogene* **20**, 7223-7233.

Kamitani, T., Kito, K., Nguyen, H. P., Wada, H., Fukuda-Kamitani, T. and Yeh, E. T. (1998). Identification of three major sentrinization sites in PML. *J. Biol. Chem.* **273**, 26675-26682.

Kentsis, A., Gordon, R. E. and Borden, K. L. (2002). Self-assembly properties of a model RING domain. *Proc. Natl. Acad. Sci. USA* **99**, 667-672.

Kentsis, A. and Borden, K. L. (2004). Physical mechanisms and biological significance of supramolecular protein self-assembly. *Curr. Protein Pept. Sci.* **5**, 125-134.

Kiesslich, A., von Mikecz, A. and Hemmerich, P. (2002). Cell cycle-dependent association of PML bodies with sites of active transcription in nuclei of mammalian cells. *J. Struct. Biol.* **140**, 167-179.

Koken, M. H. M., Puvion-Dutilleul, F., Guillemin, M. C., Viron, A., Linares-Cruz, G., Stuurman, N., de Jong, L., Szostecki, C., Calvo, F., Chomienne, C. et al. (1994). The t(15;17) translocation alters a nuclear body in a retinoic acid-reversible fashion. *EMBO J.* **13**, 1073-1079.

Kruhlak, M. J., Lever, M. A., Fischle, W., Verdin, E., Bazett-Jones, D. P. and Hendzel, M. J. (2000). The mobility of the GFP:ASF splicing factor in live cells. *J. Cell Biol.* **150**:41-51.

Kumar, P. P., Bischof, O., Purbey, P. K., Notani, D., Urlaub, H., Dejean. A. and Galande, S. (2007). Functional interaction between PML and SATB1 regulates chromatin-loop architecture and transcription of the MHC class I locus. *Nat. Cell Biol.* **9**, 45-56.

Lallemand-Breitenbach, V., Zhu, J., Puvion, F., Koken, M., Honore, N., Doubeikovsky, A., Duprez, E., Pandolfi, P. P., Puvion, E., Freemont, P. et al. (2001). Role of promyelocytic leukemia (PML) sumolation in nuclear body formation, 11S proteasome recruitment, and As2O3-induced PML or PML/retinoic acid receptor alpha degradation. *J. Exp. Med.* **193**, 1361-1371.

Lamond, A. I. and Earnshaw, W. C. (1998). Structure and function in the nucleus. *Science* **280**, 547-553.

Lanctôt, C., Cheutin, Z., Cremer, M., Cavalli, G. and Cremer, T. (2007). Dynamic genome architecture in the nuclear space: regulation of gene expression in three dimensions. *Nat. Rev. Genet.* **8**, 104-115.

Le X. F., Yang, P. and Chang, K. S. (1996). Analysis of the growth and transformation suppressor domains of promyelocytic leukemia gene, PML. *J. Biol. Chem*. **271**, 130-135.

Lin, D. Y., Huang, Y. S., Jeng, J. C., Kuo, H. Y., Chang, C. C., Chao, T. T., Ho, C. C., Chen, Y. C., Lin, T. P., Fang, H. I. et al. (2007). Role of SUMO-interacting motif in Daxx SUMO modification, subnuclear localization, and repression of sumoylated transcription factors. *Mol. Cell*. **24**, 341-354.

Maul, G. G., Yu, E., Ishov, A. M. and Epstein, A. L. (1995). Nuclear domain 10 (ND10) associated proteins are also present in NBs and redistribute to hundreds of nuclear sites after stress. *J. Cell. Biochem*. **59**, 498-513.

Maul, G. G., Negorev, D., Bell, P. and Ishov, A. M. (2000). Properties and assembly mechanisms of ND10, PML bodies, or PODs. *J. Struct. Biol.* **129**, 278-287.

Melnick, A. and Licht, J. D. (1999). Deconstructing a disease: RAR, its fusion partners, and their roles in the pathogenesis of acute promyelocytic leukemia. *Blood* **93**, 3167-3215.

Misteli, T. (2008). Physiological importance of RNA and protein mobility in the cell nucleus *Histochem. Cell Biol.* **129**, 5-11.

Mu, Z. M., Chin, K. V., Liu, J. H., Lozano, G. and Chang, K. S. (1994). PML, a growth suppressor disrupted in acute promyelocytic leukemia. *Mol. Cell. Biol*. **14**, 6858-6867.

Naka, K., Ikeda, K. and Motoyama, N. (2002). Recruitment of NBS1 into PML oncogenic domains via interaction with SP100 protein. *Biochem. Biophys. Res. Commun.* **299**, 863-871.

Negorev, D. and Maul, G. G. (2001). Cellular proteins localized at and interacting within ND10/PML NBs/PODs suggest functions of a nuclear depot. *Oncogene* **20**, 7234-7242.

Negorev, D., Ishov, A. M. and Maul, G. G. (2001). Evidence for separate ND10-binding and homo-oligomerization domains of Sp100. *J. Cell Sci*. **114**, 59-68.

Phair, R. D. and Misteli, T. (2000). High mobility of proteins in the mammalian cell nucleus. *Nature* **404**, 604-609.

Platani, M., Goldberg, I., Lamond, A. I. and Swedlow, J. R. (2002). Cajal Body dynamics and association with chromatin are ATP-dependent. *Nat. Cell Biol*. **4**, 502-508.

Quimby, B. B., Yong-Gonzalez, V., Anan, T., Strunnikov, A. V. and Dasso, M. (2006). The promyelocytic leukemia protein stimulates SUMO conjugation in yeast. *Oncogene* **25**, 2999-3005.

Reymond, A., Meroni, G., Fantozzi, A., Merla, G., Cairo, S., Luzi, L., Riganelli, D., Zanaria, E., Messali, S., Cainarca, S. et al. (2001). The tripartite motif family identifies cell compartments. *EMBO J.* **20**, 2140-2051.

Rockel, T. D., Stuhlmann, D. and von Mikecz, A. (2005). Proteasomes degrade proteins in focal subdomains of the human cell nucleus. *J. Cell Sci*. **118**, 5231-5242.

Saitoh, N., Uchimura, Y., Tachibana, T., Sugahara, S., Saitoh, H. and Nakao, M. (2006). In situ SUMOylation analysis reveals a modulatory role of RanBP2 in the nuclear rim and PML bodies. *Exp. Cell Res*. **312**, 1418-1430.

Sanz, M. M., Proytcheva, M., Ellis, N. A., Holloman, W. K. and German, J. (2000). BLM, the Bloom's syndrome protein, varies during the cell cycle in its amount, distribution, and co-localization with other nuclear proteins. *Cytogenet. Cell Genet*. **91**, 217-223.

Saxton, M. J. (2001). Anomalous subdiffusion in fluorescence photobleaching recovery: a Monte Carlo study. *Biophys. J.* **81**, 2226-2240.

Schmiedeberg, L., Weisshart, K., Diekmann, S., Hoerste, G. M. and Hemmerich, P. (2004). High- and low-mobility populations of HP1 in heterochromatin and mammalian cells. *Mol. Biol. Cell.* **15**, 2819-2833.

Seeler, J. S. and Dejean, A. (2001). SUMO: of branched proteins and nuclear bodies. *Oncogene* **20**, 7243-7249.

Seeler, J. S., Marchio, A., Sitterlin, D., Transy, C. and Dejean, A. (1998). Interaction of SP100 with HP1 proteins: a link between the promyelocytic leukemia-associated nuclear bodies and the chromatin compartment. *Proc. Natl. Acad. Sci. USA* **95**, 7316-7321.

Shen, T. H., Lin, H. K., Scaglioni, P. P., Yung, T. M. and Pandolfi, P. P. (2006). The mechanisms of PML-nuclear body formation. *Mol. Cell.* **24**, 331-339.

Shiels, C., Islam, S. A., Vatcheva, R., Sasieni, P., Sternberg, M. J., Freemont, P. S. and Sheer, D. (2001). PML bodies associate specifically with the MHC gene cluster in interphase nuclei. *J. Cell Sci.* **14**, 3705-3716.

Song, J., Durrin, L. K., Wilkinson, T. A., Krontiris, T. G. and Chen, Y. (2004). Identification of a SUMO-binding motif that recognizes SUMO-modified proteins. *Proc. Natl. Acad. Sci. USA.* **101**, 14373-14378.

Sprague, B. L. and McNally, J. G. (2005). FRAP analysis of binding: proper and fitting. *Trends Cell Biol*. **15**, 84-91.

Sternsdorf, T., Jensen, K. and Will, H. (1997). Evidence for covalent modification of the nuclear dot-associated proteins PML and Sp100 by PIC1/SUMO-1. *J. Cell Biol.* **139**, 1621-1634.

Sternsdorf, T., Jensen, K., Reich, B., and Will, H. (1999). The nuclear dot protein sp100, characterization of domains necessary for dimerization, subcellular localization, and modification by small ubiquitin-like modifiers. *J. Biol. Chem.* **274**, 12555-12566.

Sternsdorf, T., Gostissa, M., Sirma, H., Del Sal, G., Ruthard, M., Schmitz, M. L., Will, H. and Hofmann, T. G. (2005). PML nuclear bodies: Cellular function and disease association. In *Visions of the Cell Nucleus* (ed. P. Hemmerich and S. Diekmann). California: American Scientific Publishers.

Swaminathan, R., Hoang, C. P. and Verkman, A. S. (1997). Photobleaching recovery and anisotropy decay of green fluorescent protein GFP-S65T in solution and cells: cytoplasmic viscosity probed by green fluorescent protein translational and rotational diffusion. *Biophys. J.* **72**, 1900-1907.

Wachsmuth, M. Waldeck. W. and Langowski, J. (2000). Anomalous diffusion of fluorescent probes inside living cell nuclei investigated by spatially-resolved fluorescence correlation spectroscopy. *J. Mol. Biol.* **298**, 677-689.

Weidtkamp-Peters, S., Weisshart, K., Schmiedeberg, L. and Hemmerich, P. (2008). Fluorescence correlation spectroscopy to assess the mobility of nuclear proteins. *Methods Mol. Biol.* (in press).

Weis, K., Rambaud, S., Lavau, C., Jansen, J., Carvalho, T., Carmo-Fonseca, M., Lamond, A. and Dejean, A. (1994). Retinoic acid regulates aberrant nuclear localization of PML-RAR alpha in acute promyelocytic leukemia cells. *Cell* **76**, 345-356.

Wiesmeijer, K., Molenaar, C., Bekeer, I. M., Tanke, H. J. and Dirks, R. W. (2002). Mobile foci of Sp100 do not contain PML: PML bodies are immobile but PML and Sp100 proteins are not. *J. Struct. Biol*. **140**, 180-188.

Wu, L. (2007). Role of the BLM helicase in replication fork management. *DNA Repair* **6**, 936-944.

Xu, Z. X., Zou, W. X., Lin, P. and Chang K. S. (2005). A role for PML3 in centrosome duplication and genome stability. *Mol. Cell.* **17**, 721-732

Zhong, S., Muller, S., Ronchetti, S., Freemont, P. S., Dejean, A. and Pandolfi, P. P. (2000). Role of SUMO-1-modified PML in nuclear body formation. *Blood* **95**, 2748-2752.